Strong spin Hall effect in the antiferromagnet PtMn

Yongxi Ou, Shengjie Shi, D. C. Ralph, and R. A. Buhrman

Phys. Rev. B **93**, 220405 — Published 20 June 2016

DOI: 10.1103/PhysRevB.93.220405

Strong Spin Hall Effect in the Antiferromagnet PtMn

Yongxi Ou[1], Shengjie Shi[1], D. C. Ralph[1,2], and R. A. Buhrman[1,*]

[1]Cornell University, Ithaca, New York 14853, USA

[2]Kavli Institute at Cornell, Ithaca, New York 14853, USA

ABSTRACT

Effectively manipulating magnetism in ferromagnet (FM) thin film nanostructures with an in-plane current has become feasible since the determination of a "giant" spin Hall effect (SHE) in certain heavy metal (HM)/FM system. Recently, both theoretical and experimental reports indicate that metallic antiferromagnet (AF) materials can have both a large anomalous Hall effect (AHE) and a strong SHE. Here we report a systematic study of the SHE in PtMn with several PtMn/FM systems. By using interface engineering to reduce the "spin memory loss" we obtain, in the best instance, a spin torque efficiency $\xi_{DL}^{\mathrm{PtMn}} \equiv T_{\mathrm{int}}\theta_{SH}^{\mathrm{PtMn}}$; 0.24, where T_{int} is the effective interface spin transparency. This is more than twice the previously reported spin torque efficiency for PtMn. We also find that the apparent spin diffusion length in PtMn is surprisingly long, $\lambda_{\mathrm{s}}^{\mathrm{PtMn}} \approx 2.3\mathrm{nm}$.

* rab8@cornell.edu

The SHE in different heavy metal (HM)/ferromagnet (FM) systems [1–4] can be characterized by the spin Hall ratio (angle) $\theta_{SH} \equiv (2e/\mathrm{h})J_s/J_e$ where J_s is the transverse spin current density generated in the HM and J_e is the applied longitudinal electrical current density. Recently two new classes of heavy metal (HM) alloys, the non-collinear antiferromagnet (AF), Mn_3Ir [5–7] and Cu-Au-I type AF, $X_{50}Mn_{50}$ (X=Fe, Pd, Ir, and Pt) [8–11] have been reported to exhibit SHE as spin current sources, with an internal $\theta_{SH}^{\mathrm{PtMn}} \approx 0.125$ for PtMn [10], opening up a new area in the rapidly advancing field of "antiferromagnet spintronics" [12–17]. To date research on the SHE from AFs has utilized the implicit assumption that there is no interfacial spin flip scattering or "spin memory loss" (SML) [18] when the spin current traverses the interface to apply a torque to the FM. However the existence of a large SML at some Pt/FM interfaces, together with the negative enthalpy of formation of Mn with both Fe and Ni [19] that can promote interface intermixing, raises the question whether there may also be a significant SML at PtMn/FM interfaces, which would mean that the internal $\theta_{SH}^{\mathrm{PtMn}}$ within PtMn could actually be much higher than previously reported.

We performed a systematic study of the SHE in several PtMn/FM systems employing spin-torque ferromagnetic resonance (ST-FMR) [20] on in-plane magnetized (IPM) FM layers and the harmonic response (HR) Hall-effect measurements [21,22] on FM layers with perpendicular magnetic anisotropy (PMA). We also studied samples where a thin (0.25 nm – 0.8 nm) Hf layer is inserted between the PtMn and the FM to suppress strong SML at the interface [23]. We find ξ_{DL} to vary significantly with both the deposition order for a given PtMn/FM system and between the different FM systems, but to be relatively consistent between IPM and PMA samples with the same constituents. We also obtained robust current-induced switching in these PMA samples demonstrating the potential for utilizing PtMn in perpendicular

magnetic tunneling junction (p-MTJ) and three-terminal device applications.

We first fabricated a series of IPM PtMn/Co bilayer samples by sputter deposition for ST-FMR measurement of the *anti-damping* and *field-like* spin torque efficiencies, ξ_{DL} and ξ_{FL}. Because the order in which the HM and FM layers are deposited affected ξ_{DL} in a previous Pt/Co study [24] , we grew the PtMn/Co multilayers in both the "standard order" (SO) ||Ta(1.5)/PtMn(8)/Co(t_{Co})/MgO(1.6)/Ta(1.5) (series A) and in the "reversed order" (RO) ||MgO(1.6)/Co(t_{Co})/PtMn(8)/MgO(1.6)/Ta(1.5) (series B) (number in parenthesis is thickness in nm), where "||" means Si/SiO_2 substrate. All samples in this work were prepared by direct current (DC) sputtering (with RF magnetron sputtering for the MgO layer) in a deposition chamber with a base pressure $< 8\times10^{-8}$ Torr. The DC sputtering condition is 2mTorr Ar pressure, 30 watts power and low deposition rates (Ta: 0.0142 nm/s, PtMn: 0.0189 nm/s, FeCoB: 0.0064 nm/s, Co: 0.0066 nm/s). The PtMn alloy is deposited from a 2-inch planar $Pt_{50}Mn_{50}$ target, resulting in a polycrystalline PtMn layer with a predominately fcc (111) structure [25]. We utilized a Ta seeding layer as a template for smoothing the growth of the PtMn for all the standard stacking order samples. All samples have a Ta(1.5) top layer to provide an oxidized protection layer for the stack. We annealed the samples twice at $115\ ^{\circ}C$ for 1 min as part of the photolithography process. The magnetic properties of the samples, including the magnetization and dead layer thickness, were characterized by vibrating sample magnetometry (VSM), so that t_{FM}^{eff} in our study here is the effective thickness of the FM layer after subtracting the dead layer thickness.

The ST-FMR measurement schematic is illustrated in Fig. 1a. The RF current is input via the Pt contact into the samples and the signal is measured by lock-in detection. In this technique we

obtain the FMR spin torque efficiency ξ_{FMR} that is obtained from the ratio of the symmetric and antisymmetric components of anisotropic magnetoresistance response at the ferromagnetic resonance [24]. The symmetric part is proportional to the *anti-damping* torque and the antisymmetric part is due to the sum of the Oersted field torque and the *field-like* torque. Figure 1b shows the results ξ_{FMR} as a function of Co thickness t_{Co} for both the standard (main) and reversed (inset) order samples. For the SO PtMn/Co samples, the spin current in the PtMn layer generates a significant *field-like* torque in addition to the *anti-damping* torque and consequently ξ_{FMR} varies significantly with thickness [24,25]. By plotting $1/\xi_{FMR}$ *vs.* $1/t_{\mathrm{Co}}$, ξ_{DL} can be determined from the $1/t_{\mathrm{Co}} = 0$ intercept and the *field-like* spin torque efficiency ξ_{FL} can be determined from the slope of the plot, provided ξ_{FL} is effectively independent of t_{Co} [25]. For the reversed order Co/PtMn samples $\xi_{FMR}(\approx \xi_{DL})$ is essentially constant *vs.* t_{Co}, indicating ξ_{FL} is negligible (Fig. 1b inset). From this we obtain $\xi_{DL} = 0.16 \pm 0.01$ and $\xi_{FL} = -0.040 \pm 0.008$ for the SO samples and $\xi_{DL}(\text{average}) = 0.19 \pm 0.02$ and ξ_{FL} ; 0 for the RO samples (The positive sign for ξ_{DL} corresponds to the same sign of the anti-damping torque as for Pt. The minus sign for ξ_{FL} indicates that the *field-like* effective field is *opposite* to the Oersted field.)

To further confirm this result with another FM material and to examine the PtMn SHE in structures with PMA, which we were not able to obtain with PtMn/Co bilayers, we replaced Co with $Fe_{60}Co_{20}B_{20}$ (FeCoB) for the FM layer. First we fabricated two IPM series of PtMn/FeCoB bilayers samples, a SO series (C): ||Ta(1.5)/PtMn(8)/FeCoB(t_{FeCoB})/MgO(1.6)/Ta(1.5) and a RO series (D): ||MgO/FeCoB(t_{FeCoB})/PtMn(8)/MgO(1.6)/Ta(1.5). In Fig. 1c we show $1/\xi_{FMR}$ vs. $1/t_{\mathrm{FeCoB}}^{\mathrm{eff}}$ as obtained for these two sets of samples. From the linear fits to the plots we obtained

$\xi_{DL} = 0.096 \pm 0.003$, $\xi_{FL} = -0.043 \pm 0.003$ for the SO series (C) samples and

$\xi_{DL} = 0.174 \pm 0.004$, $\xi_{FL} = -0.036 \pm 0.002$ for the RO series (D) samples.

We also fabricated a SO series (E) of ||Ta(1.5)/PtMn(8)/FeCoB(t_{FeCoB})/MgO(1.6)/Ta(1.5) with a thinner FM range of $0.4\mathrm{nm} < t_{\mathrm{FeCoB}} < 1.5\mathrm{nm}$, the mid-range of which exhibited PMA without any high temperature annealing [25]. The highest out-of-plane anisotropy field $H_{an} \approx 1.8\,\mathrm{kOe}$ was achieved with $t_{\mathrm{FeCoB}} \approx 0.8\mathrm{nm}$, which allows us to perform HR measurement of the efficiency of the spin torques exerted on the perpendicularly magnetized FM. Using the measurement protocol of Ref.[21,22] on Hall-bar samples with dimensions $5 \times 60\,\mu\mathrm{m}$, the results were $\xi_{DL} = 0.11 \pm 0.02$ and $\xi_{FL} = -0.04 \pm 0.02$, in accord with the ST-FMR values obtained via ST-FMR from the IPM series (C) samples with the same layer structure but thicker FeCoB.

Recent work [23,26] has shown that the insertion of a thin layer of amorphous Hf between FeCoB and the HM in a spin Hall device structure can substantially enhance the PMA. Such a thin Hf (≤ 0.5 nm) layer does not strongly attenuate the spin current, but it does substantially reduce the interfacial contribution to damping that is typically seen in FM/Pt systems. This can be understood as the HM/Hf(~0.5)/FeCoB structure having a smaller SML than that of the seemingly simpler HM/FeCoB bilayer. At the same time we have determined that our amorphous Hf layer does not provide, by itself, any observable spin-orbit torque under our deposition conditions [26]. Since our SO PtMn/FeCoB structures appear to have a quite significant SML, we fabricated a ||Ta(1.5)/PtMn(8)/Hf(0.25)/FeCoB(0.8)/MgO(1.6)/Ta(1.5) sample (F) to determine if an ultra-thin Hf insertion layer could be efficacious in this system for enhancing spin transmission and thus ξ_{DL}. This sample also exhibits PMA without any high-temperature annealing, and using the HR method we measured an exceptionally high damping-

like spin torque efficiency $\xi_{DL} = 0.24 \pm 0.03$. Considering that because of the spin back flow effect, not all of the spin current generated within the PtMn will act on the FM [24,27], this result indicates that the internal spin Hall ratio is $\theta_{SH}^{\mathrm{PtMn}} > 0.24$. We summarize the anti-damping torques for series (A)-(F) in Table I.

To determine the spin diffusion length $\lambda_s^{\mathrm{PtMn}}$ of our PtMn films we then fabricated a set of samples, series (G), with the multilayer stack being ||Ta(1)/PtMn(t_{PtMn})/Hf(0.8)/FeCoB(0.7)/MgO, where t_{PtMn} ranged from 2 to 8 nm. The thicker Hf spacer promotes strong PMA, with an anisotropy field $H_{an} \approx 1\mathrm{Tesla}$ over the full range of PtMn thicknesses studied without annealing. In Fig. 2a we show the results of the HR measurements of *anti-damping* like effective field per unit applied electric field $\Delta H_{DL} / E$ as a function of t_{PtMn}. Because there is no spin-orbit torque arising from the Hf layer as we have determined in our case, it can be shown within a spin diffusion model that [25]:

$$\frac{\Delta H_{DL}}{E} = \frac{\sigma_{SH}}{4\pi M_s t_{FM}^{\mathrm{eff}}} \frac{G_A}{G_{\mathrm{PtMn}} \tanh(t_{\mathrm{PtMn}} / \lambda_s^{\mathrm{PtMn}}) + G_B} (1 - \mathrm{sech}(t_{\mathrm{PtMn}} / \lambda_s^{\mathrm{PtMn}})) \qquad (1)$$

where $4\pi M_s$ is the magnetization, t_{FM}^{eff} is the effective thickness of the FM layer excluding the dead layer and d_{PtMn} is the thickness of the PtMn, σ_{SH} is the spin Hall conductivity of PtMn ($\sigma_{SH} = \sigma_{\mathrm{PtMn}} \theta_{SH}^{\mathrm{PtMn}} \mathrm{h} / (2e)$), $G_{\mathrm{PtMn}} \equiv \sigma_{\mathrm{PtMn}} / \lambda_s^{\mathrm{PtMn}}$ is the spin conductance of PtMn and G_A and G_B are parameters depending on the Hf spacer and spin mixing conductance at the Hf/FeCoB interface.

Figure 2a shows a fit of Eq. (1) to the series (G) results, which gives a spin diffusion length of PtMn $\lambda_{\mathrm{PtMn}} = 2.1\mathrm{nm}$. Our result is much larger than the value 0.5 nm previously

reported [8] from inverse spin Hall effect (ISHE) measurements on NiFe/PtMn . We note that recent work has shown that a significant SML layer in the Co/Pt bilayer system can affect the estimation of λ_s in an ISHE measurements [18]. The lower anti-damping spin torque efficiency that we find without the Hf layer, which is similar to that found in the previous ISHE study [8], suggests that there is also a significant SML in those PtMn/FM cases, perhaps due to reaction of a component of the FM with Mn at PtMn/FM interface.

We should also note that Eq. (1) assumes a constant spin diffusion length that is independent of t_{PtMn}. This is not necessarily the case if the PtMn resistivity ρ_{PtMn} varies with film thickness over the range that we are employing and the Elliot-Yafet spin scattering mechanism dominates, where $\lambda_s^{\mathrm{PtMn}} \propto 1/\rho_{\mathrm{PtMn}}$. Figure 2b shows the measured resistivity of the PtMn thin layers as a function of t_{PtMn}, which is clearly not a constant. Considered this effect, we can use a "rescaling" method introduced in Ref.[27] to fit our data in Fig. 2a, which yields $\lambda_s^{\mathrm{PtMn}} = 2.3\mathrm{nm}$ for the bulk spin diffusion length [25]. This analysis yields a spin conductance for PtMn $G_{\mathrm{PtMn}} = 1/(\lambda_s^{\mathrm{PtMn}}\rho_{\mathrm{PtMn}}) = 0.37\times10^{15}\,\Omega^{-1}\mathrm{m}^{-2}$, considerably lower than that reported [28] for Pt, $G_{\mathrm{Pt}} = 1.3\times10^{15}\,\Omega^{-1}\mathrm{m}^{-2}$ (see also references cited in Ref.[27]). This low PtMn spin conductance could be advantageous in reducing the spin back-flow at an ideal (no SML) PtMn/FM interface (see Ref. [24] and references cited therein).

To demonstrate that PtMn can be used as the source of spin-transfer torque for high-efficiency magnetic switching, we performed current-induced switching with a Hall bar structure (schematic in Fig. 3a) using an as-deposited ||Ta(1)/PtMn(4)/Hf(0.5)/FeCoB(0.8)/MgO/Ta(1.5) sample (H) that had strong PMA, and that exhibited sharp and abrupt magnetic switching in its anomalous Hall signal under an out of plane field as shown in Fig. 3b. (Based on HR

measurements, this sample had $\xi_{DL} \approx 0.10$, consistent with the spin attenuation effect of the thicker Hf layer and the reduced spin current from the thinner (4nm) than optimal PtMn.) An in-plane field $H_x \geq 50$Oe and collinear to the current flow was required to allow the current to switch the magnetization deterministically, which indicates the existence a weak Dzyaloshinskii-Moriya interaction (DMI) at the Hf/FeCoB interface and a reversal process that proceeds by domain nucleation followed by spin-torque-driven domain expansion [29]. A typical current switching loop is shown in Fig. 3c, as obtained with $H_y = 200$ Oe. Figure 3d shows the spin-torque current switching phase diagram of the same sample (here 2 mA corresponds to a current density 9×10^6 A/cm^2 in PtMn). Of course the Hf insertion layer removes the possibility of exchange coupling between the PtMn and the FeCoB, which could add an additional and possibly useful aspect to the simple spin torque switching behavior reported here. We will discuss the switching behavior of PtMn/FM structures with PMA elsewhere.

The value $\xi_{DL} = 0.096 \pm 0.003$ that we obtained from our in-plane magnetized SO PtMn/FeCoB samples is quite similar to that previously reported from inverse spin Hall effect and ST-FMR measurements on in-plane magnetized PtMn/$Ni_{80}Fe_{20}$ bilayers ($\theta_{SH}^{PtMn} \approx 0.086$) [10,8]. Also the value for ξ_{FL} that we obtain for this set of PtMn/FeCoB samples is comparable to that reported in Ref. [10] from the shift of the resonance field due to a DC current applied during the FMR measurement of the PtMn/$Ni_{80}Fe_{20}$ system. In strong contrast to previous results, our values of ξ_{DL} are much higher in our RO PtMn/FeCoB samples and in both versions (SO and RO) of the PtMn/Co sample series. This strongly suggests that a significant SML forms when either FeCoB or $Ni_{80}Fe_{20}$ is sputter deposited onto PtMn, but that a weaker SML is the result when Co is deposited onto PtMn. For both Co and FeCoB we find that the

weakest SML effect occurs when the deposition order is reversed, *i.e.* in the RO samples. We take this as indicating different degrees of undesirable intermixing in the two deposition orders. For the PMA PtMn/FeCoB/MgO samples that were deposited in the standard order, ξ_{FL} is quite similar to that measured for the SO samples in the case where the FeCoB layers are thicker and hence magnetized in-plane. However by introducing an ultrathin Hf layer between the PtMn and FeCoB layers, which also enhances the PMA, the SML is greatly suppressed and we obtain $\xi_{DL} = 0.24 \pm 0.03$. This sets only a lower bound on the internal spin Hall ratio of the PtMn $\theta_{SH}^{\mathrm{PtMn}}$. Since it is reasonable to expect some remnant SML and/or spin backflow effect at this hybrid interface, further efforts to engineer the PtMn/FM interface could result in even higher values of the PtMn spin torque efficiency.

The spin diffusion length of PtMn determined in our measurement is also longer than the previously reported value (<1nm) [8]. We tentatively attribute this to the previous study being sensitive to the formation of a SML layer as the PtMn thickness is increased in those PtMn/$Ni_{80}Fe_{20}$ bilayers, as has recently been discussed for the Pt/Co case [18,30]. Of course it has to be considered that the PtMn thickness dependence of ξ_{DL} that we observe is due to some thickness dependent change in the electronic properties of the PtMn film rather than a thicker spin diffusion length than previously determined. It is well known that a fairly thick PtMn layer is required to produce the stable antiferromagnetic domains required for exchange biasing of an adjacent FM film. It is not clear however how this AFM stability would act to enhance the spin current that is generated by the electrical current passing the Pt ions, though we notice that there are seemingly contradicted results on the contribution of macroscopic exchange-bias on SHE in IrMn systems [6,11]. In regard to possible structural changes as a function of PtMn thickness our

X-ray diffraction studies [25] do not show any obvious crystalline structure changes for the different thicknesses of PtMn used in this study.

We can use the result for the PtMn spin conductance determined here to further examine the nature of the PtMn/FM interfaces we have studied. In the spin pumping theory [31,32] of a well-ordered HM/FM interface there is an enhancement of the magnetic damping that varies as $\Delta\alpha = (\gamma \mathrm{h}^2 / 8\pi^2 e^2 M_s t_{FM}^{\mathrm{eff}}) G_{\mathrm{eff}}^{\uparrow\downarrow}$ where the effective spin mixing conductance $G_{\mathrm{eff}}^{\uparrow\downarrow} \equiv G^{\uparrow\downarrow} / (1 + 2G^{\uparrow\downarrow} / G_{\mathrm{HM}})$, and $G^{\uparrow\downarrow}$ is the spin mixing conductance of the interface, assuming $\mathrm{Re}\, G^{\uparrow\downarrow}$? $\mathrm{Im}\, G^{\uparrow\downarrow}$ [25]. In all four IPM PtMn/FM series studied, ST-FMR measurements of $\Delta\alpha(t_{FM}^{-1})$ yielded $G_{\mathrm{eff}}^{\uparrow\downarrow} > 0.7 \times 10^{15} \Omega^{-1}\mathrm{m}^{-2}$ [25]. With $G_{\mathrm{PtMn}} = 0.37 \times 10^{15} \Omega^{-1}\mathrm{m}^{-2}$, this results in an unphysical (negative) value for $G^{\uparrow\downarrow}$, which means that there must be a significant SML at the PtMn/FM interface and/or a non-ideal damping enhancement at the other FM interface [24], neither of which is taken into account in the standard spin pumping theory. (We note that even if we use the previously reported results for PtMn [8] $\rho_{\mathrm{PtMn}} = 164 \mu\Omega\mathrm{cm}$ and $\lambda_s^{\mathrm{PtMn}} = 0.5\mathrm{nm}$ to determine the PtMn spin conductance, the $\Delta\alpha(t_{FM}^{-1})$ measurements still yield a negative result for $G^{\uparrow\downarrow}$.)

In summary, depending on the protocol for forming the PtMn/FM interface we have obtained very high *anti-damping* spin torque efficiencies ξ_{DL} from the spin Hall effect in PtMn, with the highest value $\xi_{DL} = 0.24 \pm 0.03 = T_{\mathrm{int}} \cdot \theta_{SH}^{\mathrm{PtMn}}$ being obtained with a PtMn/Hf(0.25)/FeCoB multilayer, where T_{int} is the net interface spin transparency of that particular system. Assuming that the intrinsic spin Hall effect dominates in PtMn, this result provides a lower bound for the spin Hall conductivity of PtMn $\sigma_{SH}^{\mathrm{PtMn}} = (\xi_{DL} / T_{\mathrm{int}}) \sigma_{\mathrm{PtMn}} > 1.5 \times 10^5 (\mathrm{h} / 2e) \Omega^{-1}\mathrm{m}^{-1}$, since $T_{\mathrm{int}} < 1$.

This can be compared to the lower bound that has been established for Pt, $\sigma_{SH}^{\mathrm{Pt}} > 5.9\times10^{5}(\mathrm{h}/2e)\Omega^{-1}\mathrm{m}^{-1}$ from recent measurements of ξ_{DL} in the PMA Pt/Co system [28]. Refinements that yield a higher T_{int} for PtMn/FM interfaces will result in even higher ξ_{DL}. We conclude that PtMn in particular and likely other binary Pt compounds in general are very promising candidates as spin current sources and detectors in spintronics applications in both IPM and PMA systems provided that the interface can be engineered to have a high spin transparency.

Acknowledgements

This research was supported by the Office of Naval Research, and by the NSF/MRSEC program (DMR-1120296) through the Cornell Center for Materials Research. We also acknowledge support from the NSF (Grant No. ECCS-1542081) through use of the Cornell Nanofabrication Facility/National Nanofabrication Infrastructure Network.

Y.O. and S.S. contributed equally to this work.

References

[1] I. M. Miron, G. Gaudin, S. Auffret, B. Rodmacq, A. Schuhl, S. Pizzini, J. Vogel, and P. Gambardella, Nat. Mater. **9**, 230 (2010).

[2] I. M. Miron, K. Garello, G. Gaudin, P.-J. Zermatten, M. V Costache, S. Auffret, S. Bandiera, B. Rodmacq, A. Schuhl, and P. Gambardella, Nature **476**, 189 (2011).

[3] L. Liu, O. J. Lee, T. J. Gudmundsen, D. C. Ralph, and R. A. Buhrman, Phys. Rev. Lett. **109**, 096602 (2012).

[4] L. Liu, C.-F. Pai, Y. Li, H. W. Tseng, D. C. Ralph, and R. A. Buhrman, Science **336**, 555 (2012).

[5] H. Chen, Q. Niu, and A. H. MacDonald, Phys. Rev. Lett. **112**, 017205 (2014).

[6] J. B. S. Mendes, R. O. Cunha, O. Alves Santos, P. R. T. Ribeiro, F. L. A. Machado, R. L. Rodríguez-Suárez, A. Azevedo, and S. M. Rezende, Phys. Rev. B **89**, 140406 (2014).

[7] W. Zhang, W. Han, S. Yang, Y. Sun, Y. Zhang, B. Yan, and S. S. P. Parkin, arXiv:1602.00670v1 (2016).

[8] W. Zhang, M. B. Jungfleisch, W. Jiang, J. E. Pearson, A. Hoffmann, F. Freimuth, and Y. Mokrousov, Phys. Rev. Lett. **113**, 196602 (2014).

[9] S. Fukami, C. Zhang, S. Duttagupta, A. Kurenkov, and H. Ohno, Nat. Mater. **15**, 535 (2016).

[10] W. Zhang, M. B. Jungfleisch, F. Freimuth, W. Jiang, J. Sklenar, J. E. Pearson, J. B. Ketterson, Y. Mokrousov, and A. Hoffmann, Phys. Rev. B **92**, 144405 (2015).

[11] V. Tshitoyan, C. Ciccarelli, A. P. Mihai, M. Ali, A. C. Irvine, T. A. Moore, T. Jungwirth, and A. J. Ferguson, Phys. Rev. B **92**, 214406 (2015).

[12] B. G. Park, J. Wunderlich, X. Martí, V. Holý, Y. Kurosaki, M. Yamada, H. Yamamoto, A. Nishide, J. Hayakawa, H. Takahashi, A. B. Shick, and T. Jungwirth, Nat. Mater. **10**, 347 (2011).

[13] V. M. T. S. Barthem, C. V Colin, H. Mayaffre, M.-H. Julien, and D. Givord, Nat. Commun. **4**, 2892 (2013).

[14] X. Marti, I. Fina, C. Frontera, J. Liu, P. Wadley, Q. He, R. J. Paull, J. D. Clarkson, J. Kudrnovský, I. Turek, J. Kuneš, D. Yi, J. H. Chu, C. T. Nelson, L. You, E. Arenholz, S. Salahuddin, J. Fontcuberta, T. Jungwirth, and R. Ramesh, Nat Mater **13**, 367 (2014).

[15] T. Satoh, R. Iida, T. Higuchi, M. Fiebig, and T. Shimura, Nat. Photon. **9**, 25 (2014).

[16] S.-H. Yang, K.-S. Ryu, and S. Parkin, Nat. Nanotechnol. **10**, 221 (2015).

[17] T. Jungwirth, X. Marti, P. Wadley, and J. Wunderlich, Nat. Nanotechnol. **11**, 231 (2016).

[18] J.-C. C. Rojas-Sánchez, N. Reyren, P. Laczkowski, W. Savero, J.-P. P. Attané, C. Deranlot, M. Jamet, J.-M. M. George, L. Vila, and H. Jaffrès, Phys. Rev. Lett. **112**, 106602 (2014).

[19] S. V. Meschel, P. Nash, and X. Q. Chen, J. Alloys Compd. **492**, 105 (2010).

[20] L. Liu, T. Moriyama, D. C. Ralph, and R. A. Buhrman, Phys. Rev. Lett. **106**, 036601 (2011).

[21] U. H. Pi, K. Won Kim, J. Y. Bae, S. C. Lee, Y. J. Cho, K. S. Kim, and S. Seo, Appl. Phys. Lett. **97**, 162507 (2010).

[22] J. Kim, J. Sinha, M. Hayashi, M. Yamanouchi, S. Fukami, T. Suzuki, S. Mitani, and H. Ohno, Nat. Mater. **12**, 240 (2013).

[23] M.-H. Nguyen, K. X. Nguyen, D. A. Muller, D. C. Ralph, R. A. Buhrman, and C.-F. Pai, Appl. Phys. Lett. **106**, 222402 (2015).

[24] C.-F. Pai, Y. Ou, L. H. Vilela-Leão, D. C. Ralph, and R. A. Buhrman, Phys. Rev. B **92**, 064426 (2015).

[25] See Supplementary Materials for more information.

[26] C.-F. Pai, M.-H. Nguyen, C. Belvin, L. H. Vilela-Leão, D. C. Ralph, and R. A. Buhrman, Appl. Phys. Lett. **104**, 082407 (2014).

[27] W. Zhang, W. Han, X. Jiang, S.-H. Yang, and S. S. P. Parkin, Nat. Phys. **11**, 496 (2015).

[28] M.-H. Nguyen, D. C. Ralph, and R. A. Buhrman, Phys. Rev. Lett. **116**, 126601 (2016).

[29] O. J. Lee, L. Q. Liu, C. F. Pai, Y. Li, H. W. Tseng, P. G. Gowtham, J. P. Park, D. C. Ralph, and R. A. Buhrman, Phys. Rev. B **89**, 024418 (2014).

[30] Y. Liu, Z. Yuan, R. J. H. Wesselink, A. A. Starikov, and P. J. Kelly, Phys. Rev. Lett. **113**, 207202 (2014).

[31] Y. Tserkovnyak, A. Brataas, and G. Bauer, Phys. Rev. Lett. **88**, 117601 (2002).

[32] Y. Tserkovnyak, A. Brataas, and G. Bauer, Phys. Rev. B **66**, 224403 (2002).

Figure 1

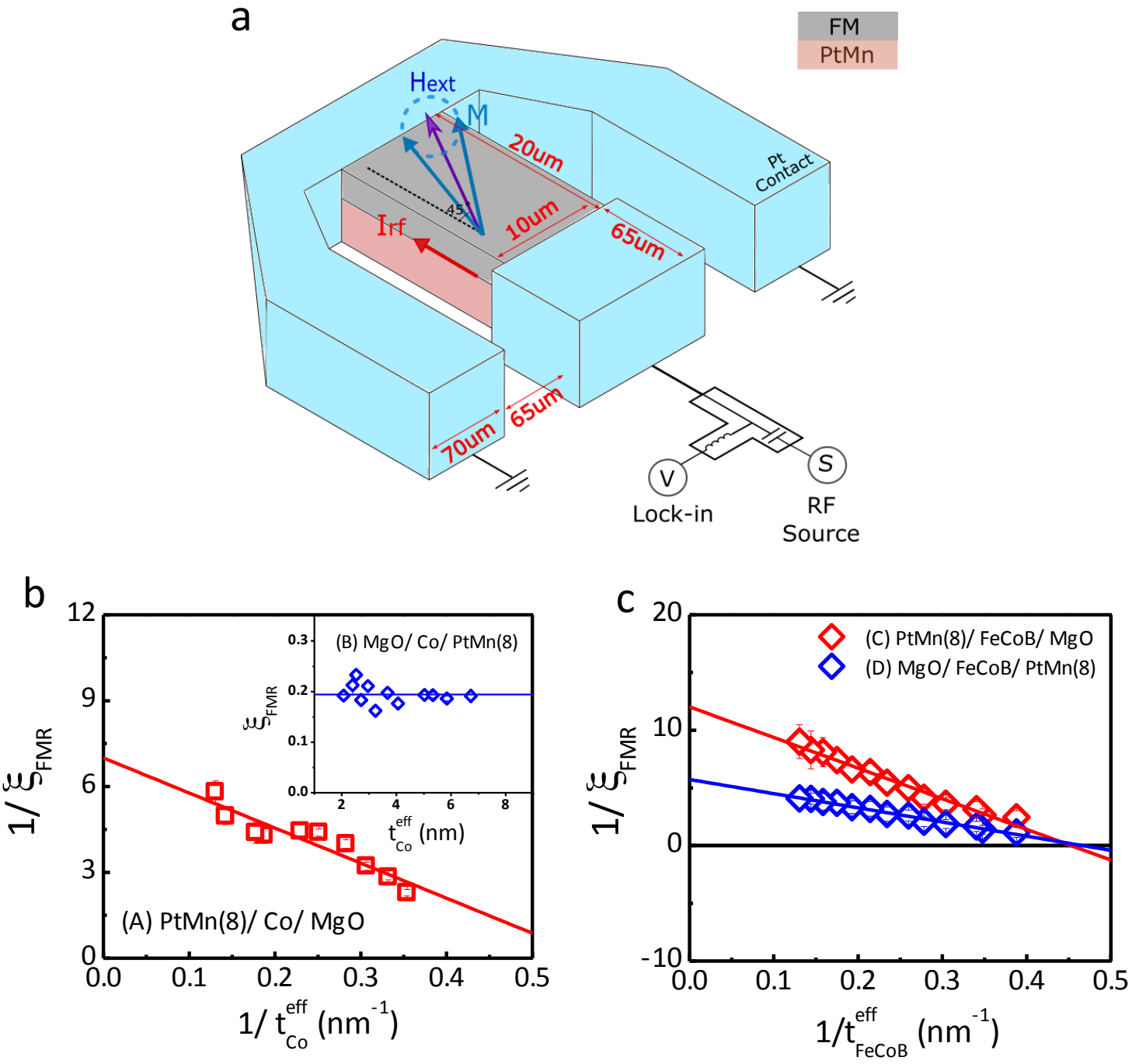

FIG. 1. (a) Schematic of ST-FMR measurement. The Pt contact is 150nm thick. (b) The inverse of the ST-FMR measured spin torque efficiency, $1/\xi_{FMR}$, as a function of the inverse of the effective thickness for the Co series (A) samples (red squares). Inset: ξ_{FMR} as a function of $t_{\mathrm{Co}}^{\mathrm{eff}}$

for series (B) samples (blue squares). (c) $1/\xi_{FMR}$ as a function of $1/t_{\mathrm{FeCoB}}^{\mathrm{eff}}$ for the series (C) (red squares) and series (D) (blue squares) samples.

Figure 2

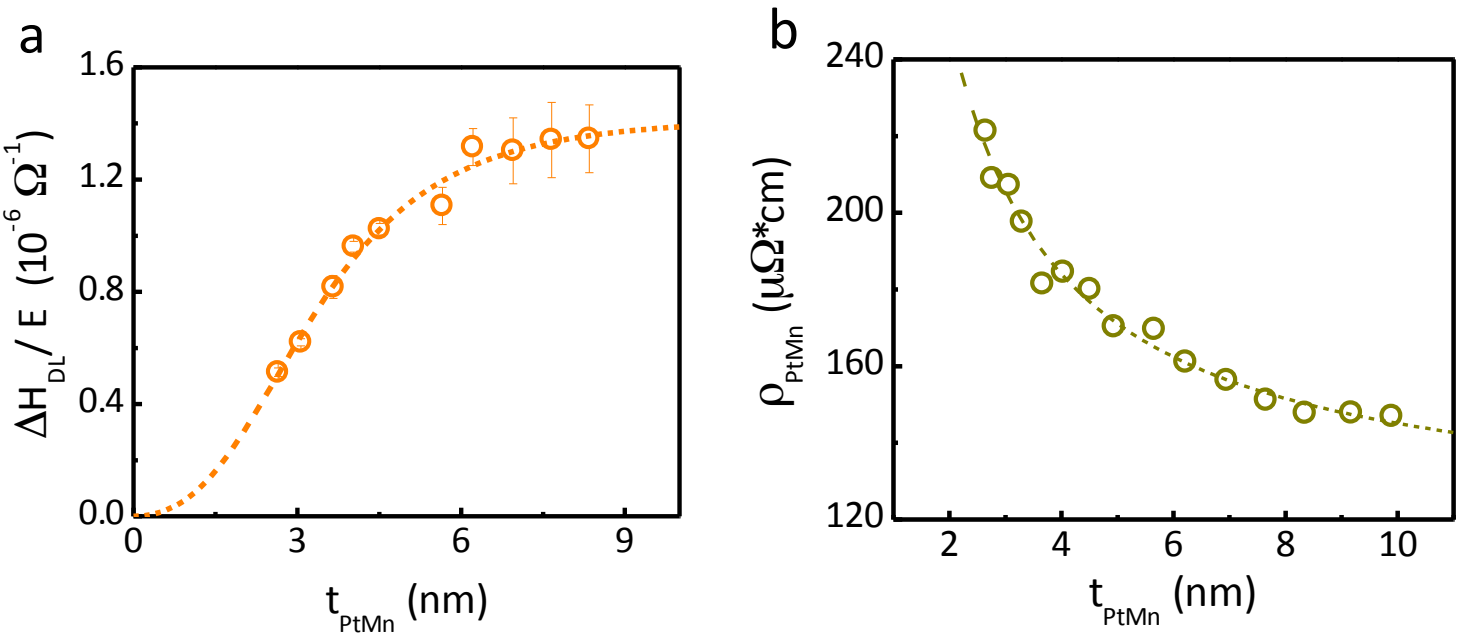

FIG. 2. (a) Damping-like effective field per unit applied electric field for the series (G) samples as a function of PtMn thickness t_{PtMn}. (b) Average resistivity of different thicknesses of PtMn. The dash line is a fit of the empirical function $\rho_0 + \rho_s / t_{\mathrm{PtMn}}$ to the data, where ρ_0 and ρ_s are represent the bulk and interfacial scattering contributions to the resistivity.

Figure 3

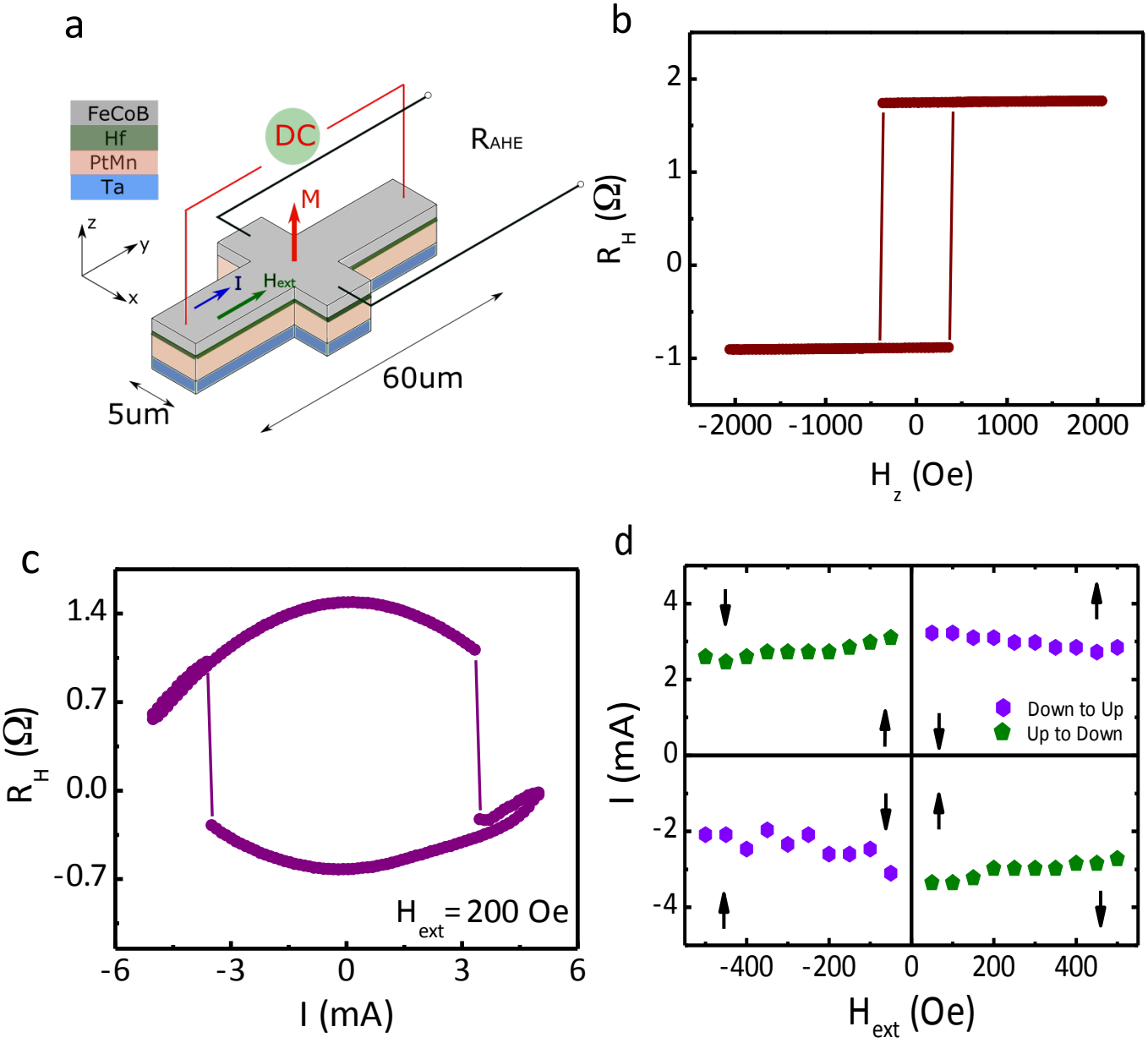

FIG. 3. (a) Schematic of the Hall-bar samples used to study field- and current-induced switching. (b) Magnetic field switching of a series (H) sample with the field perpendicular to the sample plane. (c) Current-induced switching of the same sample with an external magnetic field (200 Oe)

applied in-plane along the current direction. (d) Phase diagram of the current-induced switching behavior.